Available online at www.sciencedirect.com
ScienceDirect
European Journal of Mechanics A/Solids 25 (2006) 595–616

# Bifurcation phenomena in non-smooth dynamical systems

R.I. Leine [a,*], D.H. van Campen [b]

[a] *IMES–Center of Mechanics, ETH Zentrum, CH-8092 Zürich, Switzerland*
[b] *Eindhoven University of Technology, Department of Mechanical Engineering, P.O. Box 513, 5600 MB Eindhoven, The Netherlands*

Received 13 February 2006; accepted 21 April 2006

Available online 7 July 2006

**Abstract**

The aim of the paper is to give an overview of bifurcation phenomena which are typical for non-smooth dynamical systems. A small number of well-chosen examples of various kinds of non-smooth systems will be presented, followed by a discussion of the bifurcation phenomena in hand and a brief introduction to the mathematical tools which have been developed to study these phenomena. The bifurcations of equilibria in two planar non-smooth continuous systems are analysed by using a generalised Jacobian matrix. A mechanical example of a non-autonomous Filippov system, belonging to the class of differential inclusions, is studied and shows a number of remarkable discontinuous bifurcations of periodic solutions. A generalisation of the Floquet theory is introduced which explains bifurcation phenomena in differential inclusions. Lastly, the dynamics of the Woodpecker Toy is analysed with a one-dimensional Poincaré map method. The dynamics is greatly influenced by simultaneous impacts which cause discontinuous bifurcations.


*Keywords:* Measure differential inclusions; Bifurcation; Friction; Impact; Discontinuity

## 1. Introduction

The dynamics of non-smooth systems is a relatively young research field. A look at the programs of international conferences from the past decade reveals a rapidly increasing interest in non-smooth systems. It is perhaps not exaggerated to state that it is nowadays fashion to study non-smooth systems. One reason for this great interest is, that non-smooth models appear in many different disciplines. Mechanical engineers study stick–slip oscillations in systems with dry friction and the dynamics of impact phenomena with unilateral constraints. Electrical circuits contain diodes and transistors, which ideally behave in a non-smooth way. Control theorists have to deal with switching control laws. Similar problems of switching systems arise in air traffic management, economic models of markets and scheduling of automated railway systems. Although these examples come from very different fields, the mathematical structure and the related questions of interest are very similar. In particular, the time evolution is often described by non-smooth differential equations or (measure) differential inclusions. We distinguish three types of non-smooth dynamical systems:

* Corresponding author.
*E-mail addresses:* remco.leine@imes.mavt.ethz.ch (R.I. Leine), D.H.v.Campen@tue.nl (D.H. van Campen).

0997-7538/$ – see front matter 
doi:10.1016/j.euromechsol.2006.04.004

1. *Non-smooth continuous systems* which are described by differential equations with a continuous but non-differentiable right-hand side.
2. *Filippov systems* which are described by differential equations with a discontinuous right-hand side, but with a time-continuous state. Systems of this type can be transformed into differential inclusions with a set-valued right-hand side by using Filippov's convex method (Filippov, 1988).
3. *Systems which expose discontinuities in time of the state*, such as impacting systems with velocity reversals and electrical systems with resets. This type of systems can be described by measure differential inclusions.

Nonlinear dynamical systems can possess equilibria and periodic solutions as well as other special solutions of the system such as quasi-periodic solutions and chaotic attractors/repellors, which can all be either stable or unstable, and determine the long-term dynamics of the system. Here, we will consider equilibria and periodic solutions of non-smooth dynamical systems. It is often desirable to know how the equilibria and periodic solutions of a system alter when a parameter of the system is varied. The number and stability of equilibria/periodic solutions can change at a certain critical parameter value. Loosely speaking, this qualitative change in the structural behaviour of the system is called *bifurcation*, a word introduced by H. Poincaré. Various definitions of bifurcation exist in literature, which all agree for smooth dynamical systems, but become distinct when applied to non-smooth systems (Leine and Nijmeijer, 2004). The most intuitive definition of bifurcation is to say that a bifurcation occurs when the number of equilibria/periodic solutions changes at a critical parameter value, being what Poincaré originally meant with the word bifurcation. In this paper, we will adopt this definition as it can be unambiguously applied to non-smooth systems.

The theory of bifurcations in smooth dynamical systems is well understood, but much less is known about bifurcations in non-smooth systems although currently a lot of research is being done on this topic. Bifurcations of equilibria of non-smooth continuous systems are related to bifurcations of fixed points of piecewise smooth maps. Nusse and York (1992) study so-called 'border-collision bifurcations' of two-dimensional non-smooth discrete maps. Many publications deal with bifurcations in non-smooth systems of Filippov-type. Published bifurcation diagrams are often constructed from data obtained by brute force techniques and only show branches of stable periodic solutions (see for instance, Begley and Virgin, 1998; Blazejczyk-Okolewska and Kapitaniak, 1996; Dankowicz and Nordmark, 2000; Galvanetto and Knudsen, 1997; Hinrichs et al., 1998; Kunze and Küpper, 1997; Oancea and Laursen, 1998; Popp et al., 1995). Bifurcation diagrams calculated with path-following techniques show bifurcations to unstable periodic solutions but the bifurcations behave as conventional bifurcations in smooth systems (Stelter and Sextro, 1991; Van de Vrande et al., 1999). Experimental bifurcation diagrams of non-smooth systems compared with numerical results using the path-following technique can be found in Mihajlović et al. (2004) (dry friction) and in Van de Vorst (1996) (impact). Few publications show non-conventional bifurcations in Filippov systems which cannot be understood with the classical bifurcation theory for smooth systems, see for instance Elmer (1997), Casini and Vestroni (2004), Yoshitake and Sueoka (2000). Non-conventional bifurcations in a double friction oscillator are studied in a rather complete way by Casini and Vestroni (2004). Yoshitake and Sueoka (2000) address Floquet theory and remark that the Floquet multipliers 'jump' at the bifurcation point. Feigin (1978; 1995) considers Poincaré maps of Filippov systems, which are locally piecewise continuous maps and introduced the term 'C-bifurcation' for the non-conventional bifurcations which occur in periodic solutions of Filippov systems. The work of Feigin has been extended by di Bernardo et al. (1999; 2002).

Non-conventional bifurcations of periodic solutions of Filippov systems are furthermore studied in previous works of the authors (Leine et al., 2000; Leine, 2000; Leine and Van Campen, 2002; Leine et al., 2002; Leine and Nijmeijer, 2004), in which non-conventional bifurcations are addressed as *discontinuous bifurcations*. The basic idea is that Floquet multipliers of Filippov systems can 'jump' when a parameter of the system is varied, as was noticed in Yoshitake and Sueoka (2000). If a Floquet multiplier jumps through the unit circle in the complex plane then a discontinuous bifurcation can be encountered. In the work of Leine et al. it is explained how the discontinuous bifurcations come into being through jumps of the fundamental solution matrix, which leads to a generalised Floquet theory. Moreover, it is shown how discontinuous bifurcations are related to conventional bifurcations in smooth systems.

Another type of non-conventional bifurcation is the 'grazing bifurcation' which occurs in impacting systems. A grazing bifurcation can occur in a rigid multibody system with unilateral contacts if the pre-impact velocity becomes zero. Bifurcations in impacting systems are studied by Brogliato (1999), Ivanov (1996), Foale and Bishop (1994), Leine et al. (2003), Meijaard (1996), Molenaar et al. (2001), Nordmark (1997), Peterka (1996).

The aim of the present paper is to give an overview of bifurcation phenomena which are typical for non-smooth dynamical systems as they do not occur in smooth dynamical systems. This paper will neither discuss in detail the mathematical prerequisites for non-smooth analysis, nor give an in-depth discussion of a rigorous bifurcation theory for a certain class of non-smooth systems, as has been done in Leine and Nijmeijer (2004). The aim of the present paper is far more modest and a different approach is chosen. Instead, only a small number of well-chosen examples of various kinds of systems will be studied, followed by a discussion of the bifurcation phenomena in hand and a brief introduction to the mathematical tools which have been developed to study these phenomena. This approach has clear benefits for the non-specialist reader and allows to discuss a wide class of systems in a less rigorous and more accessible way.

Two examples of non-smooth continuous systems will be studied in Section 2. These examples demonstrate that bifurcations in non-smooth systems are sometimes similar to known bifurcations from classical bifurcation theory in smooth vector fields but can also be completely different. Section 3 discusses the dynamics of a block-on-belt system, that undergoes forced stick–slip oscillations. This example of a non-autonomous Filippov system shows a remarkable bifurcation behaviour and demonstrates the use of generalised Floquet multipliers. Subsequently, the complex dynamics of the Woodpecker Toy, which is governed by frictional impact, is analysed in Section 4 with a one-dimensional Poincaré map method. Conclusions that can be drawn from these examples are given in Section 5.

## 2. Non-smooth continuous systems

In this section we will discuss two examples of differential equations

$$\dot{\boldsymbol{x}} = \boldsymbol{f}(\boldsymbol{x}, \mu) \tag{1}$$

for which the right-hand side is continuous but non-differentiable on one or more switching boundaries $\Sigma_i$. The right-hand side is dependent on a constant parameter $\mu$, which plays the role of a bifurcation parameter. The chosen examples are planar systems which, although they appear to be very simple, show a remarkable bifurcation behaviour.

First, consider the planar non-smooth continuous system

$$\begin{aligned} \dot{x}_1 &= x_2, \\ \dot{x}_2 &= -x_2 - \frac{3}{2}|x_2 - \mu| - x_1, \end{aligned} \tag{2}$$

which has one switching boundary $\Sigma = \{(x_1, x_2) \in \mathbb{R}^2 \mid x_2 - \mu = 0\}$ on which the right-hand side is non-differentiable. The system has only one equilibrium point

$$x_1 = -\frac{3}{2}|\mu|, \qquad x_2 = 0, \tag{3}$$

which exists for all $\mu \in \mathbb{R}$. The system is piecewise linear and the equilibrium is not located on the switching boundary if $\mu \neq 0$. The dynamics in the vicinity of the equilibrium for $\mu < 0$ is therefore determined by the Jacobian matrix $\boldsymbol{J}_+$ with eigenvalues $\lambda^+_{1,2}$, and for $\mu > 0$ by the Jacobian matrix $\boldsymbol{J}_-$ with eigenvalues $\lambda^-_{1,2}$:

$$\begin{aligned} \boldsymbol{J}_+ &= \begin{bmatrix} 0 & 1 \\ -1 & -\frac{5}{2} \end{bmatrix}, \quad \lambda^+_1 = -2, \quad \lambda^+_2 = -\frac{1}{2}, \quad \mu < 0, \\ \boldsymbol{J}_- &= \begin{bmatrix} 0 & 1 \\ -1 & \frac{1}{2} \end{bmatrix}, \quad \lambda^-_{1,2} = \frac{1}{4} \pm \frac{1}{4}\sqrt{15}\,\mathrm{i}, \quad \mu > 0. \end{aligned} \tag{4}$$

Looking at the eigenvalues, we see that the equilibrium is a stable node for $\mu < 0$ and an unstable focus for $\mu > 0$ and therefore loses stability at $\mu = 0$. The phase plane of system (2) is shown in Fig. 1 for $\mu = -1$, showing a stable node, and for $\mu = 1$, showing an unstable focus and a stable limit cycle. Because the vector field is non-smooth but still continuous, we can use the generalised differential of Clarke (Clarke et al., 1998; Leine and Nijmeijer, 2004) to set up a generalised Jacobian matrix. The generalised Jacobian matrix of the system is

$$\boldsymbol{J}(\boldsymbol{x}, \mu) = \begin{bmatrix} 0 & 1 \\ -1 & -1 - \frac{3}{2}\,\mathrm{Sign}(x_2 - \mu) \end{bmatrix}, \tag{5}$$

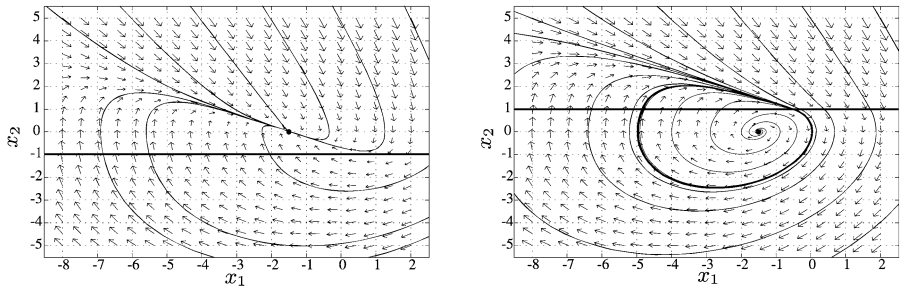


Fig. 1. Discontinuous Hopf bifurcation of system (2).

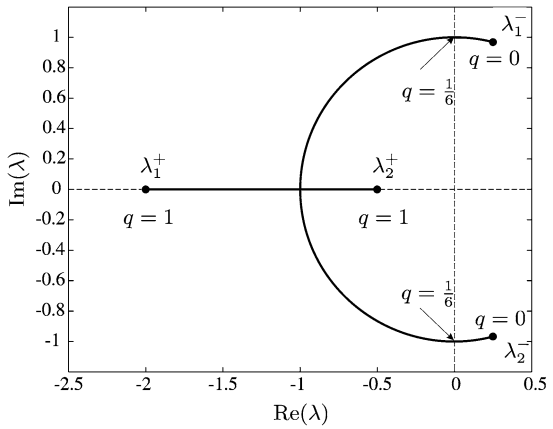


Fig. 2. Eigenvalue-path of the discontinuous Hopf bifurcation of system (2).

where $\mathrm{Sign}(x)$ denotes the set-valued sign-function. The generalised Jacobian at the equilibrium point $x_1 = x_2 = 0$ for $\mu = 0$ can be expressed as the set-valued matrix $\boldsymbol{J}(\boldsymbol{0}) = \{\boldsymbol{J}_q,\ q \in [0,1]\}$ with $\boldsymbol{J}_q = q\boldsymbol{J}_+ + (1-q)\boldsymbol{J}_-$. The two eigenvalues are therefore set-valued at the equilibrium point for $\mu = 0$ and form a one-dimensional path in the complex plane parameterised by the auxiliary variable $q$ and given by $\lambda_i = \{\lambda_{qi},\ q \in [0,1]\}$ with $\lambda_{qi} = \mathrm{eig}\,\boldsymbol{J}_q$ for $i = 1, 2$:

$$\lambda_{q1,2} = \begin{cases} \frac{1}{4} - \frac{3}{2}q \pm \frac{1}{4}\mathrm{i}\sqrt{-(1-6q)^2 + 16}, & q \leqslant \frac{5}{6}, \\ \frac{1}{4} - \frac{3}{2}q \pm \frac{1}{4}\sqrt{(1-6q)^2 - 16}, & q > \frac{5}{6}. \end{cases} \tag{6}$$

The path of the eigenvalues is depicted in Fig. 2. The eigenvalues cross the imaginary axis for $q = \frac{1}{6}$, which causes a Hopf bifurcation phenomenon. We call this a discontinuous Hopf bifurcation, as the associated eigenvalues *jump* as a complex conjugated pair through the imaginary axis. The phase plane in Fig. 1 for $\mu = 1$ shows indeed a stable limit cycle, created by the discontinuous Hopf bifurcation. Using a non-smooth version of Bendixson's criterion it is possible to prove that the condition

$$\mathrm{trace}(\boldsymbol{J}_+)\,\mathrm{trace}(\boldsymbol{J}_-) < 0 \tag{7}$$

is a necessary condition for the existence of a limit cycle in this class of systems. Furthermore, it is possible to prove that if a discontinuous Hopf bifurcation occurs, in the sense that a limit cycle is created, then a pair of complex conjugated eigenvalues *must* jump through the imaginary axis. See Leine and Nijmeijer (2004) for theorems and proofs. The bifurcation in hand is discontinuous, but very much behaves like a classical Hopf bifurcation which can occur in a smooth dynamical system. The following example, however, shows a more unexpected bifurcation behaviour.

Consider the planar non-smooth continuous system

$$\begin{aligned} \dot{x}_1 &= x_1 + 2|x_1| + x_2, \\ \dot{x}_2 &= x_1 + 2|x_1| + \frac{1}{2}x_2 + \mu, \end{aligned} \tag{8}$$

which is piecewise linear and has a single switching boundary $\Sigma = \{\boldsymbol{x} \in \mathbb{R}^2 \mid x_1 = 0\}$. For $\mu < 0$, the system (8) has two distinct equilibria

$$\begin{aligned} &\text{equilibrium 1:} \quad x_1 = -\frac{2}{3}\mu, \quad x_2 = 2\mu, \\ &\text{equilibrium 2:} \quad x_1 = 2\mu, \qquad x_2 = 2\mu, \end{aligned} \tag{9}$$

while it has no equilibria for $\mu > 0$. The generalised Jacobian matrix of the system is

$$\boldsymbol{J}(x_1) = \begin{bmatrix} 1 + 2\,\mathrm{Sign}(x_1) & 1 \\ 1 + 2\,\mathrm{Sign}(x_1) & \frac{1}{2} \end{bmatrix}, \tag{10}$$

which takes a constant value $\boldsymbol{J}_\pm$ at each side of the switching boundary $\Sigma$:

$$\boldsymbol{J}_- = \begin{bmatrix} -1 & 1 \\ -1 & \frac{1}{2} \end{bmatrix} \quad \text{for } x_1 < 0, \quad \lambda_{1,2} = -\frac{1}{4} \pm \mathrm{i}\sqrt{\frac{7}{16}}, \tag{11}$$

$$\boldsymbol{J}_+ = \begin{bmatrix} 3 & 1 \\ 3 & \frac{1}{2} \end{bmatrix} \quad \text{for } x_1 > 0, \quad \lambda_{1,2} = \frac{7}{4} \pm \sqrt{\frac{73}{16}} \approx \{-0.386, 3.886\}. \tag{12}$$

The generalised Jacobian at the bifurcation point $\boldsymbol{x} = \boldsymbol{0}$ is the closed convex hull of the Jacobians on each side of the switching boundary

$$\boldsymbol{J}(\boldsymbol{0}) = \overline{\mathrm{co}}(\boldsymbol{J}_-, \boldsymbol{J}_+) = \big\{(1-q)\boldsymbol{J}_- + q\boldsymbol{J}_+, \ \forall q \in [0,1]\big\}. \tag{13}$$

The eigenvalues $\lambda_{1,2}$ of $\boldsymbol{J}(\boldsymbol{0})$ are set-valued and form a *path* in the complex plane with $q$ as path parameter. The path of eigenvalues of the generalised Jacobian at $\boldsymbol{x} = \boldsymbol{0}$ is depicted in Fig. 3. The eigenvalues of $\boldsymbol{J}_q$ are purely imaginary for $q = \frac{1}{8}$ and one eigenvalue crosses the origin for $q = \frac{1}{4}$. The path of the eigenvalues of $\boldsymbol{J}(\boldsymbol{0})$ shows that the discontinuous bifurcation point is a *multiple crossing bifurcation*, in the sense that the eigenvalues cross the imaginary axis more than once during their jump. One might suggest that the behaviour of this multiple crossing bifurcation is the combination of two conventional bifurcations, a Hopf bifurcation and a turning point bifurcation. Fig. 4 depicts the phase plane of (8) for $\mu = -1$, $\mu = 0$ and $\mu = 1$. The two equilibria (9) are present for $\mu = -1$ of which one equilibrium is a stable focus and the other equilibrium is a saddle point. The invariant manifolds of the saddle point show an interesting behaviour. An unstable invariant half-manifold of the saddle point is spiralling towards the stable focus while one of the stable invariant half-manifolds is folded to the other stable invariant half-manifold. The two equilibria collide to one equilibrium for $\mu = 0$ and only two invariant half-manifolds (a stable and an unstable)

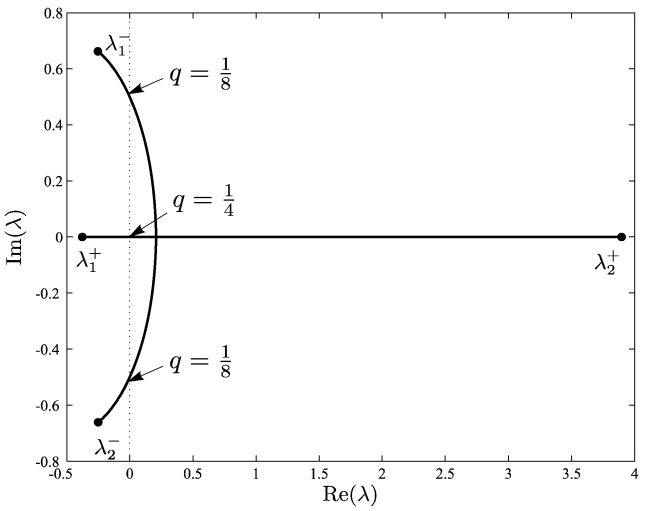


Fig. 3. Path of the eigenvalues of $\boldsymbol{J}(\boldsymbol{0})$ (13) of system (8).

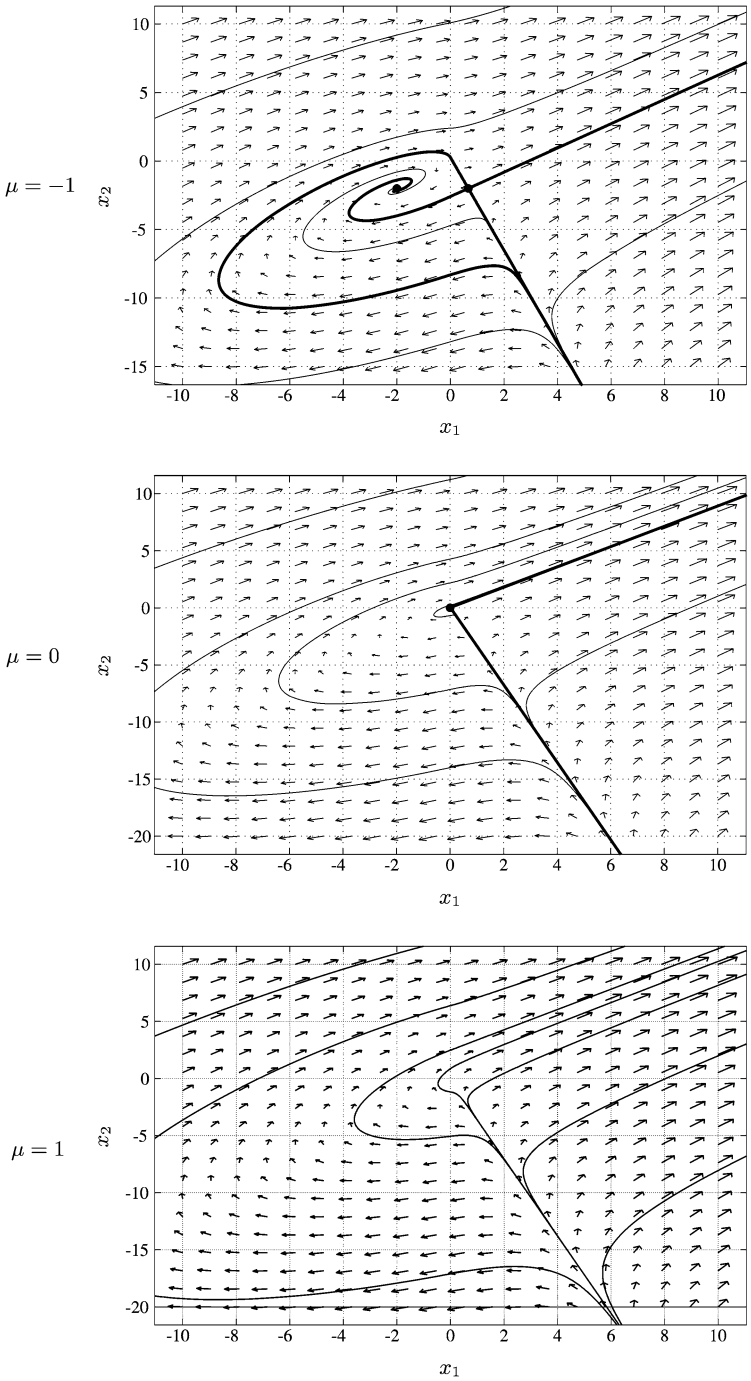


Fig. 4. Multiple crossing bifurcation of system (8).

remain. An equilibrium having only two invariant half-manifolds is a peculiarity of non-smooth continuous systems. No equilibrium or periodic solution exists for $\mu = 1$. The multiple crossing bifurcation has the structure:

$$\left.\begin{array}{l}\text{stable focus}\\ \text{saddle}\end{array}\right\} \xrightarrow{\text{multiple crossing bifurcation of (8)}} \emptyset.$$

Clearly, the behaviour of a turning point bifurcation is present in the bifurcation scenario observed in Fig. 4 (see also the Turning Point Theorem 8.9 in Leine and Nijmeijer, 2004). The bifurcation scenario does not show a creation (or

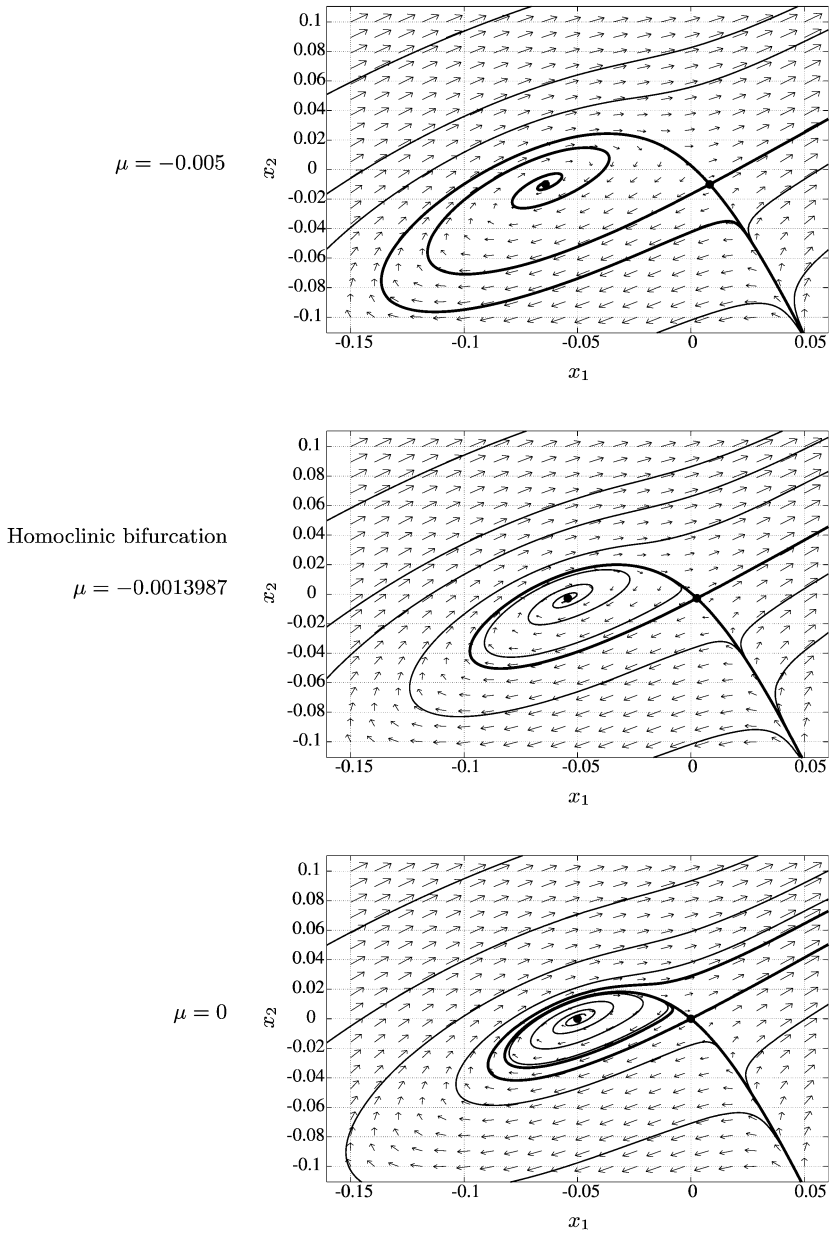


Fig. 5. Homoclinic bifurcation, system (14), $\varepsilon = 20$.

destruction) of a periodic solution under variation of $\mu$, i.e. no behaviour of a Hopf bifurcation. The multiple crossing bifurcation is therefore not simply the combination of two conventional bifurcations.

Some insight in the bifurcation behaviour depicted in Fig. 4 can be obtained by considering a smooth approximation of system (8)

$$\begin{aligned} \dot{x}_1 &= x_1 + \frac{4}{\pi}\arctan(\varepsilon x_1)x_1 + x_2, \\ \dot{x}_2 &= x_1 + \frac{4}{\pi}\arctan(\varepsilon x_1)x_1 + \frac{1}{2}x_2 + \mu. \end{aligned} \tag{14}$$

Of course, we have to keep in mind that (14) is just one particular smooth approximation of (8). Figs. 5 and 6 show the phase planes of (14) for six different values of $\mu$ in the neighbourhood of $\mu = 0$ (using $\varepsilon = 20$). Two equilibria exist

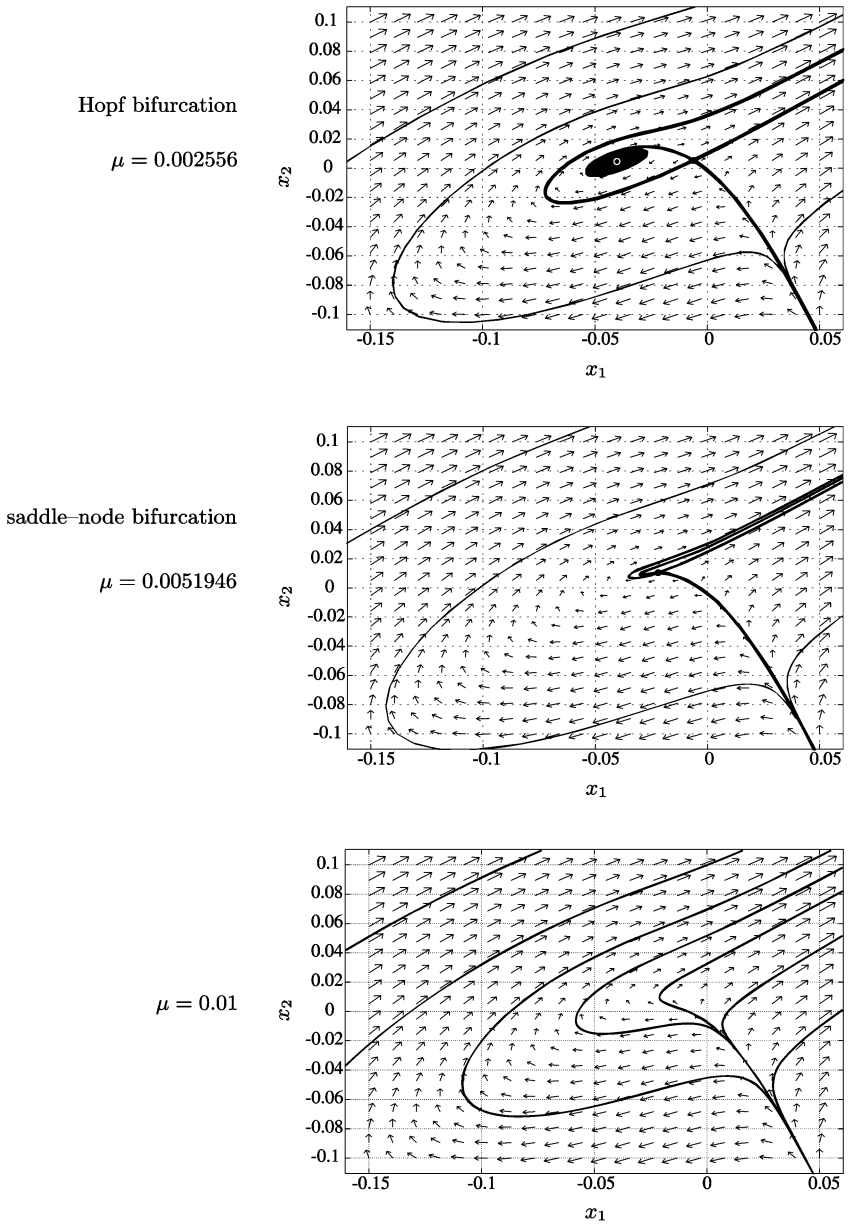


Fig. 6. Hopf and saddle–node bifurcation, system (14), $\varepsilon = 20$.

for $\mu = -0.005$ and the phase plane is very similar to the phase plane in Fig. 4 for $\mu = -1$. An unstable invariant half-manifold of the saddle point is spiralling towards the stable focus. A stable invariant half-manifold of the saddle point is very close to this spiralling unstable invariant half-manifold, turns around it and is folded towards the other stable invariant half-manifold. The stable and unstable invariant half-manifolds, already close for $\mu = -0.05$, collide for $\mu = -0.0013987$. The collision of the two invariant half-manifolds causes a homoclinic trajectory, i.e. a trajectory that connects an equilibrium point with itself. The homoclinic trajectory only exists for $\mu = -0.0013987$ and is immediately destroyed if $\mu$ is further increased. The destruction of the homoclinic trajectory causes the stable invariant half-manifold to spiral (in reverse time) around the equilibrium point, as can been seen in the phase plane for $\mu = 0$. The unstable invariant half-manifold is folded towards the other unstable invariant half-manifold of the saddle point. The behaviour of the stable and unstable invariant half-manifold is therefore inverted. This type of global bifurcation is called *homoclinic bifurcation*. The homoclinic bifurcation creates (or destroys) a periodic solution. The periodic

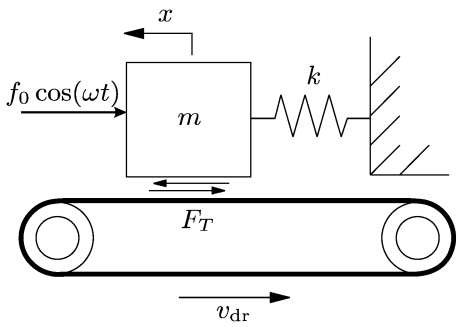


Fig. 7. The forced stick–slip system (15).

solution can be seen in the phase plane for $\mu = 0$ and forms the boundary of the two-dimensional region of attraction of the stable focus. The periodic solution is therefore an unstable limit cycle. The structure of the bifurcation scenario of Fig. 5 is summarised in the following diagram:

$$\left.\begin{array}{l}\text{stable focus}\\ \text{saddle}\end{array}\right\} \xrightarrow{\substack{\text{homoclinic}\\ \text{bifurcation}}} \begin{array}{l}\text{stable focus}\\ \text{unstable limit cycle}\\ \text{saddle}\end{array}$$

A further increase of the parameter $\mu$ diminishes the size of the periodic solution and a Hopf bifurcation occurs at $\mu = 0.002556$ (Fig. 6). The equilibrium, which is a stable focus for $\mu < 0.002556$, becomes an unstable focus after the Hopf bifurcation and turns into an unstable node after a focus-node transition. Finally, the two equilibria, being a saddle point and a node, collide and a saddle-node bifurcation takes place for $\mu = 0.0051946$. No equilibrium or periodic solution is present in the phase plane for $\mu = 0.01$. The structure of the bifurcation scenario of Fig. 6 continues the bifurcation scenario of Fig. 5. A Hopf bifurcation destroys a limit cycle and transforms a stable focus into an unstable focus, which co-exists with a saddle:

$$\left.\begin{array}{l}\text{stable focus}\\ \text{unstable limit cycle}\\ \text{saddle}\end{array}\right\} \xrightarrow{\substack{\text{Hopf}\\ \text{bifurcation}}} \begin{array}{l}\\ \text{unstable focus}\\ \text{saddle}\end{array}$$

Subsequently, the unstable focus is transformed into an unstable node and is destroyed together with the co-existing saddle by a saddle-node bifurcation:

$$\left.\begin{array}{l}\text{unstable focus}\\ \text{saddle}\end{array}\right. \xrightarrow{\substack{\text{focus-node}\\ \text{transition}}} \left.\begin{array}{l}\text{unstable node}\\ \text{saddle}\end{array}\right\} \xrightarrow{\substack{\text{saddle-node}\\ \text{bifurcation}}} \emptyset.$$

The smoothing of the non-smooth terms causes the eigenvalues to be a single-valued function of the parameter $\mu$. The multiple crossing bifurcation of (8) is therefore, for this particular choice of the smoothing function, torn apart in two conventional crossing bifurcations (a Hopf bifurcation and a saddle–node bifurcation) and a global bifurcation (a homoclinic bifurcation). The bifurcation structure of the non-smooth continuous system shows only one discontinuous multiple crossing bifurcation:

$$\left.\begin{array}{l}\text{stable focus}\\ \text{saddle}\end{array}\right\} \xrightarrow{\substack{\text{multiplecrossing}\\ \text{bifurcation}}} \emptyset$$

which replaces the complex structure of the smooth approximating system. The question rises how to name this particular multiple crossing bifurcation. The behaviour of the discontinuous bifurcation is much more complex than just the behaviour of a turning point, which is reflected by the complex structure of conventional bifurcations of the smooth approximating system (14). It has become clear that the problem of terminology is becoming extremely difficult when studying more complex bifurcations.

## 3. Filippov systems: a forced stick–slip system

In this section we study a forced stick–slip system (Fig. 7), which has been introduced by Yoshitake and Sueoka (2000) and further analysed in Leine (2000) and Leine and Nijmeijer (2004). This system is a mechanical example of a non-autonomous Filippov system, i.e. a differential inclusion with a closed convex upper semi-continuous image. A block with mass $m$, is supported by a spring $k$ to a wall and is riding on a belt which moves with the constant velocity $v_{\mathrm{dr}}$. An external force $f_0\cos(\omega t)$ is applied on the mass in horizontal direction. The friction model for the contact between block and belt is a set-valued Coulomb friction model with a Stribeck effect. The system can be expressed by the second-order differential inclusion

$$m\ddot{x} + kx = F_T(v_{\mathrm{rel}}) + f_0\cos(\omega t), \tag{15}$$

with $v_{\mathrm{rel}} = \dot{x} - v_{\mathrm{dr}}$. The set-valued friction model reads as

$$-F_T(v_{\mathrm{rel}}) \in \alpha_0\,\mathrm{Sign}(v_{\mathrm{rel}}) - \alpha_1 v_{\mathrm{rel}} + \alpha_3 v_{\mathrm{rel}}^3. \tag{16}$$

The bifurcation diagrams depicted in Figs. 8–10 were obtained numerically using the parameter values of (Yoshitake and Sueoka, 2000): $m = 1$ kg, $k = 1$ N/m, $v_{\mathrm{dr}} = 1$ m/s, $\alpha_0 = 1.5$ N, $\alpha_1 = 1.5$ Ns/m, $\alpha_3 = 0.45$ Ns$^3$/m$^3$ and $f_0 = 0.1$ N. The resonance curve of system (15) has been published in (Yoshitake and Sueoka, 2000) for $0.2 \leqslant \omega \leqslant 4$. The 1/2-subharmonic closed resonance curve is of special interest and depicted in Fig. 8(a), and an enlargement in Fig. 8(b). Solid lines indicate branches of stable periodic solutions and dashed lines indicate branches of unstable periodic solutions.

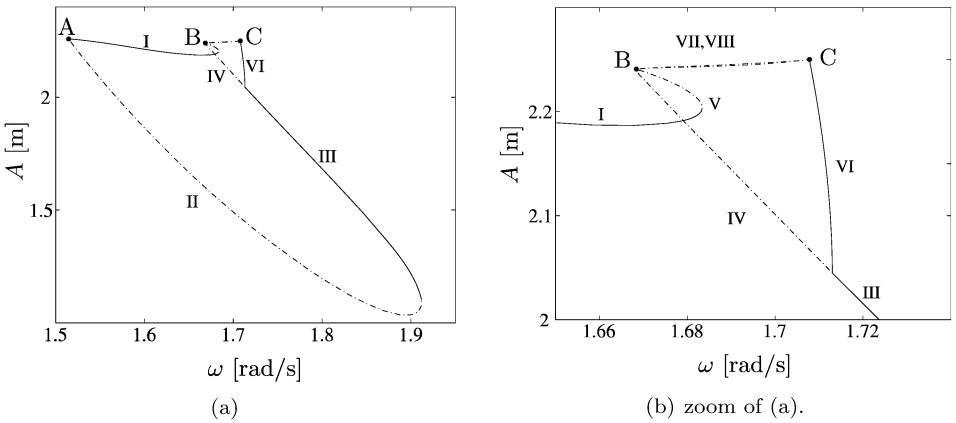


Fig. 8. Bifurcation diagram of the forced stick–slip system (15).

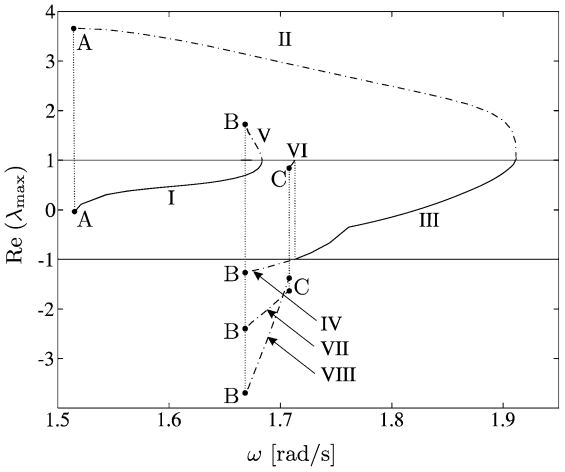


Fig. 9. Floquet multipliers of system (15).

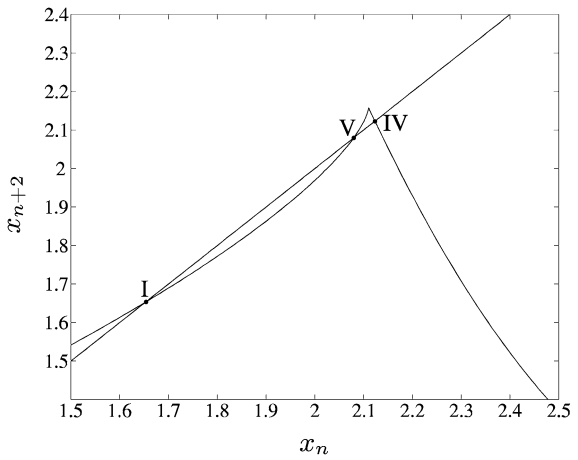


Fig. 10. Poincaré map of (15) ($\omega = 1.67587$ [rad/s]).

The stability of periodic solutions is governed by the monodromy matrix, being the fundamental solution matrix after the period time $T$. The monodromy matrix $\boldsymbol{\Phi}_T$ relates how an infinitely small perturbation $\delta\boldsymbol{x}_0$ of an initial point $\boldsymbol{x}_0$ on the periodic solution causes a final disturbance $\delta\boldsymbol{x}_T$ of the end-point $\boldsymbol{x}_T = \boldsymbol{x}_0$ of the periodic solution:

$$\delta\boldsymbol{x}_T = \boldsymbol{\Phi}_T \delta\boldsymbol{x}_0. \tag{17}$$

For smooth dynamical systems, the monodromy matrix $\boldsymbol{\Phi}_T = \boldsymbol{\Phi}(T, 0, \boldsymbol{x}_0)$ is obtained by integrating the so-called variational equation (a matrix differential equation)

$$\dot{\boldsymbol{\Phi}}(t, 0, \boldsymbol{x}_0) = \frac{\partial \boldsymbol{f}(t, \boldsymbol{x}(t))}{\partial \boldsymbol{x}} \boldsymbol{\Phi}(t, 0, \boldsymbol{x}_0), \qquad \boldsymbol{\Phi}(0, 0, \boldsymbol{x}_0) = \boldsymbol{I}, \tag{18}$$

where $\boldsymbol{x}(t)$ is the periodic solution with $\boldsymbol{x}(0) = \boldsymbol{x}_0$. However, for Filippov systems the vector field $\boldsymbol{f}(t, \boldsymbol{x})$ is discontinuous at a switching boundary $\Sigma$ and the gradient $\partial \boldsymbol{f}(t, \boldsymbol{x}(t))/\partial \boldsymbol{x}$ does therefore not exist when $\boldsymbol{x}(t) \in \Sigma$. The crossing of the switching boundary $\Sigma$ by the solution $\boldsymbol{x}(t)$ at time instance $t_p$ causes the fundamental solution matrix to jump, which we describe by a saltation matrix $\boldsymbol{S}$ (Leine and Nijmeijer, 2004)

$$\boldsymbol{\Phi}(t_p^+, 0, \boldsymbol{x}_0) = \boldsymbol{S}\boldsymbol{\Phi}(t_p^-, 0, \boldsymbol{x}_0) \tag{19}$$

with

$$\boldsymbol{S} = \boldsymbol{I} + \frac{(\boldsymbol{f}_p^+ - \boldsymbol{f}_p^-)\boldsymbol{n}^{\mathrm{T}}}{\boldsymbol{n}^{\mathrm{T}}\boldsymbol{f}_p^- + \frac{\partial h}{\partial t}(t_p, \boldsymbol{x}(t_p))} \tag{20}$$

where $\boldsymbol{f}_p^{\pm}$ are the right-hand sides before and after crossing the switching boundary, $\boldsymbol{n}$ is the normal to $\Sigma$ and $h(t, \boldsymbol{x})$ is the function which describes $\Sigma = \{\boldsymbol{x} \in \mathbb{R}^n \mid h(t, \boldsymbol{x}) = 0\}$. The fundamental solution matrix is in fact a linearisation around the periodic solution and therefore serves as a kind of Jacobian matrix. In the previous section we saw how we can generalise a Jacobian matrix around an equilibrium point to a generalised set-valued Jacobian matrix for non-smooth systems using the generalised derivative of Clarke. In the same way we can define a generalised, possibly set-valued, fundamental solution matrix. If the periodic solution touches a non-smooth point of $\Sigma$, then also the monodromy matrix will be set-valued (Leine, 2000). The periodic solution of a non-autonomous system is stable if all eigenvalues of the monodromy matrix, called Floquet multipliers, are located within the unit circle (i.e. have a complex magnitude smaller than unity). A set-valued monodromy matrix will naturally have set-valued Floquet multipliers.

The real part of the largest Floquet multiplier (in magnitude) of the branches of periodic solutions in Fig. 8 is depicted in Fig. 9. All Floquet multipliers are real except on a part of branch III near point B. Stable branches of periodic solutions are denoted by solid lines and unstable branches by dashed-dotted lines. We see that the Floquet multipliers are set-valued at the points A, B and C (indicated by dotted lines).

The 1/2-subharmonic closed resonance curve possesses several discontinuous and continuous bifurcations. Branches I–V are period-2 solutions, i.e. periodic solutions with period time $2T$. Branches VI and VII are period-4, and branch VIII is period-8. A fold bifurcation at point A connects the stable branch I to the unstable branch II. We see in Fig. 9 that the largest Floquet multiplier at point A 'jumps' through $+1$ and we call this bifurcation therefore a discontinuous fold bifurcation. The stable branch I smoothly folds into branch V and stability is exchanged. At point B, the unstable branch V is folded into the unstable branch IV *without exchanging stability*. The set-valued Floquet multiplier at point B crosses the unit circle twice as it 'jumps' from $\lambda > 1$ on branch V to $\lambda < -1$ on branch IV, i.e. the Floquet multiplier contains the points $+1$ and $-1$ on the unit circle in its set. We therefore call the associated bifurcation a multiple crossing bifurcation of a periodic solution, because the Floquet multipliers cross the unit circle more than once during their jump. The analysis of multiple crossing bifurcations of equilibria in non-smooth continuous systems makes it clear that a multiple crossing bifurcation can generally *not* be interpreted as the combination of conventional bifurcations. The fold action of the bifurcation point B in Fig. 9 is clear as the branch is folded. A conventional continuous period-doubling bifurcation causes a period-doubled branch to bifurcate from the main branch. Branches IV and V are period-2 and branch VII emanates indeed from point B and is period-4. The bifurcation at point B therefore also shows a period-doubling action. In addition, branch VIII also bifurcates from bifurcation point B and is period-8. Bifurcation point B shows the behaviour of a continuous fold and period-doubling bifurcation but also shows the creation of many more branches (chaos). Consequently, this particular multiple crossing bifurcation is not simply the combination of two conventional bifurcations.

A better understanding of the phenomenon can be obtained by looking at the Poincaré map depicted in Fig. 10. Note that the map is indeed similar to the tent map. In fact, the 'full' Poincaré map is a mapping from $\mathbb{R}^2$ to $\mathbb{R}^2$, because the system is three-dimensional, and the Poincaré map can therefore not easily be visualised. Instead, a section of this map is depicted with the displacement $x_n = x(nT)$, where $T = 2\pi/\omega$, on the abscissa and the displacement after two periods $x_{n+2}$ on the ordinate (because we study period-2 oscillations). The section of the map is such, that $\dot{x}_n$ is equal to $\dot{x}_{n+2}$. Fixed points of this reduced map are periodic solutions of period-2 (or period-1) as $x(nT) = x((n+2)T)$ holds and likewise $\dot{x}(nT) = \dot{x}((n+2)T)$. The map is calculated for $\omega = 1.67587$ [rad/s], which is just to the right of the bifurcation point B. It can be seen that there are three fixed points, which correspond to the periodic solutions at the branches I, IV and V. The map exposes a peak between the fixed points IV and V. Although this map is a section of a higher-dimensional map, the 'full' map will also be similar to the tent map.

The one-dimensional tent map has been studied thoroughly in literature (e.g., Glendinning, 1994). The tent map is a non-smooth piecewise linear version of the logistic map (both non-invertible). The logistic map is smooth and leads to a cascade of period-doublings, which is a well known route to chaos. The distance between two succeeding period-doublings is non-zero for the logistic map. An infinite number of period-doublings occur at the same bifurcation value for the tent map, which leads directly to chaos. The results on the tent map could explain the behaviour at the bifurcation point B. The similarity between the tent map and the Poincaré map suggests that there are infinitely many period-doublings. This would result in an infinite number of other unstable branches starting from point B (period-8, 16, 32, ...). A period-8 branch (VIII) starting from point B has indeed been found besides the 'expected' period-4 branch (VII). The infinitely many other branches become more unstable as their period-doubling number increases and the branches become closely located to each other, which makes it difficult to find them numerically. These facts agree with the analytical results on the tent map. Similar to the tent map, the system will (presumably) behave chaotically for $\omega$-values just to the right of point B.

A multiple crossing bifurcation of a periodic solution in a Filippov system has been discussed in this section and it has been shown that it is related to the one-dimensional tent map. It is suggested that infinitely many branches meet at the same bifurcation point and these branches are all period-doublings of the branch under bifurcation.

## 4. Systems with impact: the Woodpecker Toy

Lagrangian mechanical systems with (frictional) impact undergo discontinuities in the generalised velocities when an impact occurs and form an important subclass of systems with state discontinuities. This type of systems can be conveniently described by measure differential inclusions (Moreau, 1988b). Lagrangian mechanical systems can be expressed by a measure equation of motion (Glocker, 2001)

$$\boldsymbol{M}(\boldsymbol{q},t)\,\mathrm{d}\boldsymbol{u} - \boldsymbol{h}(\boldsymbol{q},\boldsymbol{u},t)\,\mathrm{d}t = \boldsymbol{W}_N(\boldsymbol{q},t)\,\mathrm{d}\boldsymbol{\Lambda}_N + \boldsymbol{W}_T(\boldsymbol{q},t)\,\mathrm{d}\boldsymbol{\Lambda}_T, \tag{21}$$

where $\boldsymbol{q}$ are the absolutely continuous generalised positions, and $\boldsymbol{u}$ are the generalised velocities which are assumed to be of locally bounded variation. The latter admit a differential measure $\mathrm{d}\boldsymbol{u}$ containing a Lebesgue measurable part and an atomic part accounting for the discontinuous motion. We denote by $\boldsymbol{M}(\boldsymbol{q},t)$ the symmetric positive definite mass matrix and by $\boldsymbol{h}(\boldsymbol{q},t)$ the vector of all smooth finite forces. The contact forces and impulses associated with the unilateral contacts can be decomposed in a part normal to the contact plane and a frictional part tangential to the contact plane. The generalised force directions of the normal and tangential contact efforts are stored as columns in the matrices $\boldsymbol{W}_N$ and $\boldsymbol{W}_T$. The contact effort in normal direction admits a differential measure $\mathrm{d}\boldsymbol{\Lambda}_N = \boldsymbol{\lambda}_N\,\mathrm{d}t + \boldsymbol{\Lambda}_N\,\mathrm{d}\eta$ which consists of the Lebesgue measurable forces $\boldsymbol{\lambda}_N$ and the impulses $\boldsymbol{\Lambda}_N$ and the same holds for the tangential contact efforts (Moreau, 1988a). The differential contact efforts are assumed to obey set-valued laws (Glocker, 2001) which describe the constitutive behaviour of the unilateral contact, i.e. unilaterality of the contact, friction and impact. The measure equation of motion together with set-valued constitutive laws constitute a measure differential inclusion in second-order form.

In this section we will study the dynamics of the Woodpecker Toy as a mechanical example of a system with discontinuities in the state. The Woodpecker Toy (Fig. 11) is a wooden toy with interesting dynamic behaviour, showing both impact and friction phenomena. The toy consists of a sleeve, a spring and the woodpecker. The hole in the sleeve is slightly larger than the diameter of the pole, thus allowing a kind of pitching motion interrupted by impacts with friction.

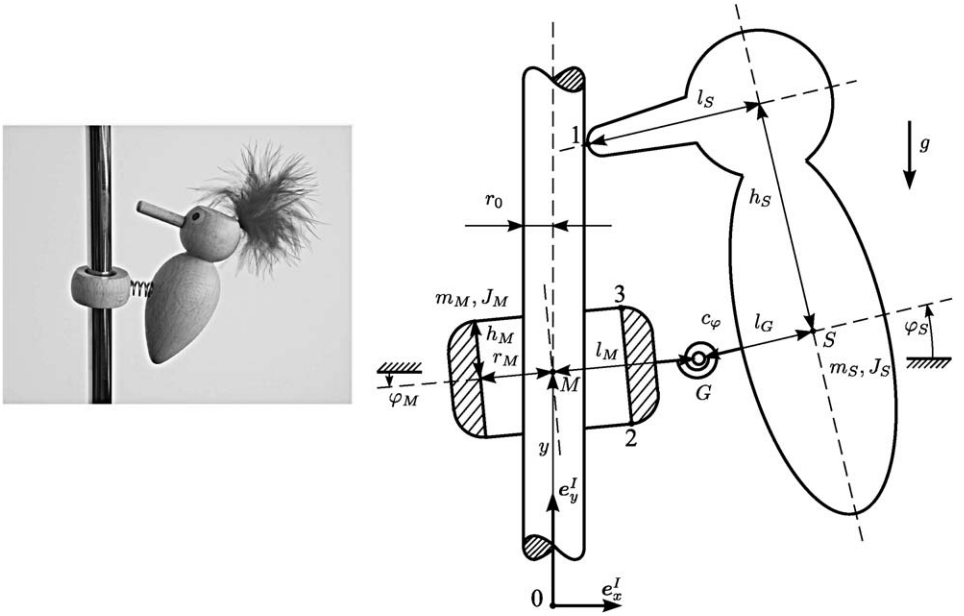


Fig. 11. Model of the Woodpecker Toy (not on scale) (Glocker, 1995).

The scientific study of this toy dates back to the beginning of the 1980s (Pfeiffer, 1984). At that time one was not able to deal with systems with impact and friction. A heuristic model was presented in (Pfeiffer, 1984), in which the friction losses were determined experimentally. The lack of a more general theory gave the onset for the work of Glocker (Glocker, 1995; Pfeiffer and Glocker, 1996), who formulated a multi-body theory for impact problems with friction using a description on force-acceleration level together with a LCP formulation of the friction and impact laws. In Glocker (1995), Pfeiffer and Glocker (1996) and Glocker and Studer (2005) a model for the Woodpecker Toy has been presented as example for the developed theory. Furthermore, the Woodpecker Toy has been studied in Glocker and Studer (2005) by using the time-stepping method, a sophisticated integration method for measure differential inclusions. A bifurcation analysis of periodic solutions in the system, based on a one-dimensional mapping, has been given in Leine et al. (2003) and will be briefly reviewed in this section.

The Woodpecker Toy is a system which can only operate in the presence of friction as it relies on combined impacts and jamming. Restitution of the beak with the pole is not essential for a periodic motion but enlarges the resemblance with the typical behaviour of a woodpecker. The motion of the toy lies in a plane, which reduces the number of degrees of freedom to model the system. The planar system (Fig. 11) possesses three degrees of freedom $\boldsymbol{q} = [\, y \quad \varphi_M \quad \varphi_S \,]^{\mathrm{T}}$, where $\varphi_S$ and $\varphi_M$ are the absolute angles of rotation of the woodpecker and the sleeve, respectively, and $y$ describes the vertical displacement of the sleeve. Horizontal displacement of the sleeve is negligible. Due to the clearance between sleeve and pole, the lower or upper edge of the sleeve may come into contact with the pole, which is modelled by constraints 2 and 3. Furthermore, contact between the beak of the woodpecker with the pole is expressed by constraint 1. The special geometry of the design enables us to assume only small deviations of the rotations. Thus a linearised evaluation of the system's kinematics is sufficient and leads to the model listed below. The mass matrix $\boldsymbol{M}$, the force vector $\boldsymbol{h}$ and the constraint vectors $\boldsymbol{w}$ follow from Fig. 11 in a straightforward manner. They are

$$\boldsymbol{M} = \begin{bmatrix} (m_S + m_M) & m_S l_M & m_S l_G \\ m_S l_M & (J_S + m_S l_M^2) & m_S l_M l_G \\ m_S l_G & m_S l_M l_G & (J_S + m_S l_G^2) \end{bmatrix}, \qquad \boldsymbol{h} = \begin{bmatrix} -(m_S + m_M) g \\ -c_\varphi(\varphi_M - \varphi_S) - m_S g l_M \\ -c_\varphi(\varphi_S - \varphi_M) - m_S g l_G \end{bmatrix},$$

$$g_{N1} = (l_M + l_G - l_S - r_0) - h_S \varphi_S, \quad g_{N2} = (r_M - r_0) + h_M \varphi_M, \quad g_{N3} = (r_M - r_0) - h_M \varphi_M,$$

$$\boldsymbol{w}_{N1} = \begin{bmatrix} 0 \\ 0 \\ -h_S \end{bmatrix}, \quad \boldsymbol{w}_{N2} = \begin{bmatrix} 0 \\ h_M \\ 0 \end{bmatrix}, \quad \boldsymbol{w}_{N3} = \begin{bmatrix} 0 \\ -h_M \\ 0 \end{bmatrix}, \tag{22}$$

$$\boldsymbol{w}_{T1} = \begin{bmatrix} 1 \\ l_M \\ l_G - l_S \end{bmatrix}, \quad \boldsymbol{w}_{T2} = \begin{bmatrix} 1 \\ r_M \\ 0 \end{bmatrix}, \quad \boldsymbol{w}_{T3} = \begin{bmatrix} 1 \\ r_M \\ 0 \end{bmatrix}.$$

For the numerical analysis of the Woodpecker Toy we consider the same data set as taken in Glocker (1995), Pfeiffer and Glocker (1996) and Glocker and Studer (2005):

Dynamics: $m_M = 0.0003$ kg; $J_M = 5.0\ 10^{-9}$ kg m$^2$; $m_S = 0.0045$ kg; $J_S = 7.0\ 10^{-7}$ kg m$^2$; $g = 9.81$ m/s$^2$;
Geometry: $r_0 = 0.0025$ m; $r_M = 0.0031$ m; $h_M = 0.0058$ m; $l_M = 0.010$ m; $l_G = 0.015$ m; $h_S = 0.020$ m; $l_S = 0.0201$ m;
Contact: $\mu_1 = \mu_2 = \mu_3 = 0.3$; $\varepsilon_{N1} = 0.5$; $\varepsilon_{N2} = \varepsilon_{N3} = 0.0$;

The motions of the sleeve and woodpecker are limited by the contacts, $|\varphi_M| \leqslant (r_M - r_0)/h_M = 0.1034$ rad and $\varphi_S \leqslant (l_M + l_G - l_S - r_0)/h_S = 0.12$ rad. The system has a stable (but non-attractive) equilibrium position, in which the woodpecker is hanging backward on the jamming sleeve, $\boldsymbol{q} = [\, y \quad -0.1034 \quad -0.2216\,]^{\mathrm{T}}$. The jamming of the sleeve with the pole at that position is only possible if $\mu_2 \geqslant 0.285$. The equilibrium point is stable but non-attractive because no damping is modelled between woodpecker and sleeve, but is asymptotically stable in practice due to ever existing dissipation in reality.

Using the above data set, the motion of the woodpecker was simulated (using an event-driven integration technique (Leine et al., 2003) as well as the time-stepping method (Glocker and Studer, 2005)) and a stable periodic solution was found with period $T = 0.1452$ s. The time histories of two periods of this periodic solution are shown in Fig. 12 and the corresponding phase space portraits are shown in Fig. 13. The numbers 1–8 correspond with the frames depicted in Fig. 14. Let $t_k$ denote the time at frame $k$. Just before $t = t_1$ the sleeve is jamming and the woodpecker is rotating upward, thereby reducing the normal force in contact 2. At $t = t_1$, the sleeve starts sliding downward, due to the reduced normal contact force, and contact is lost at $t = t_2$. In the time interval $t_2 < t < t_3$, the toy is in free fall and is quickly gaining kinetic energy. The first upper sleeve impact occurs at $t = t_3$ but the contact immediately detaches. A beak impact occurs at $t = t_4$, which changes the direction of motion of the woodpecker. The beak impact is soon followed by the second upper sleeve impact at $t = t_5$. Detachment of the upper sleeve contact occurs at $t = t_6$. The toy is again in unconstrained motion during the time interval $t_6 < t < t_7$. A high frequency oscillation can be

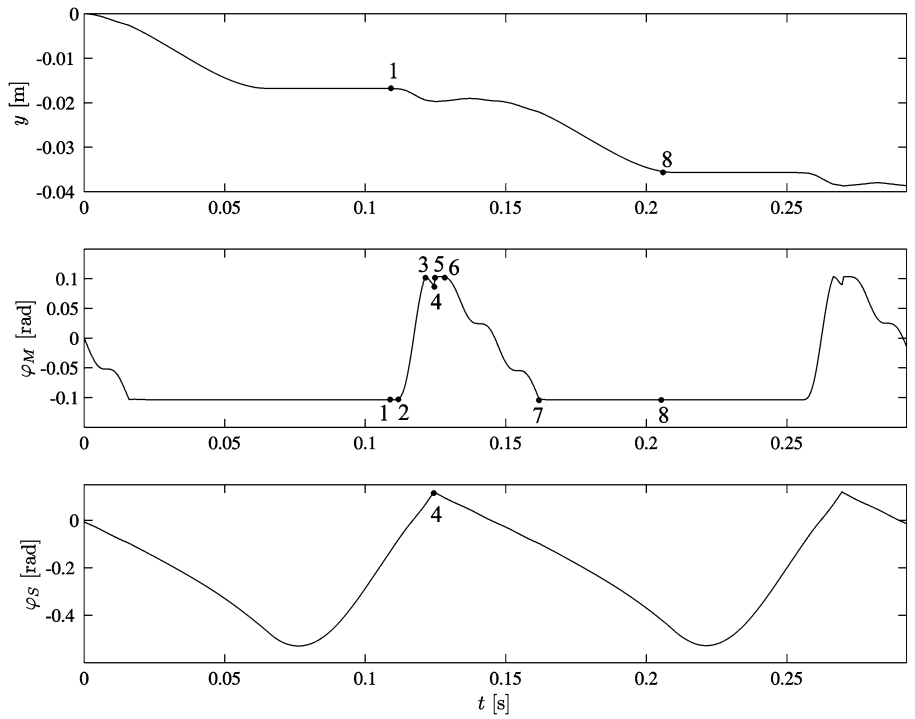


Fig. 12. Time history of the coordinates.

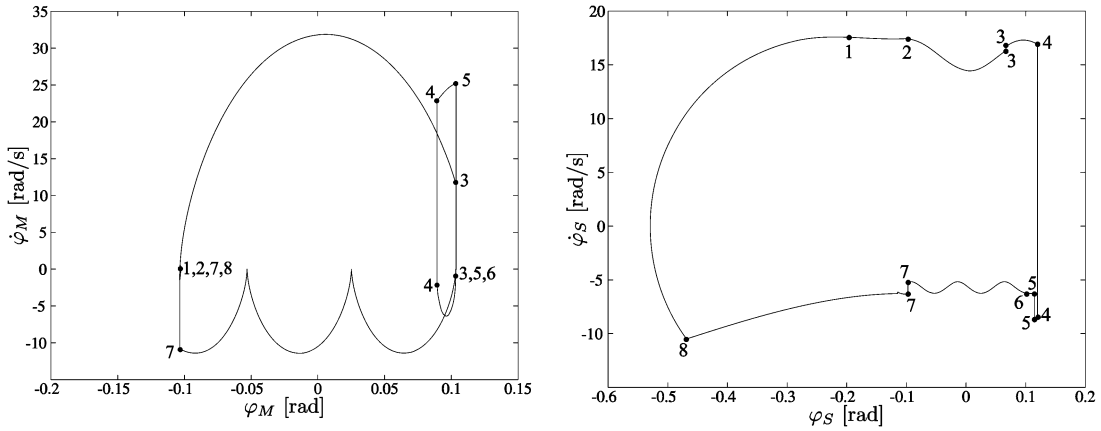


Fig. 13. Phase space portraits.

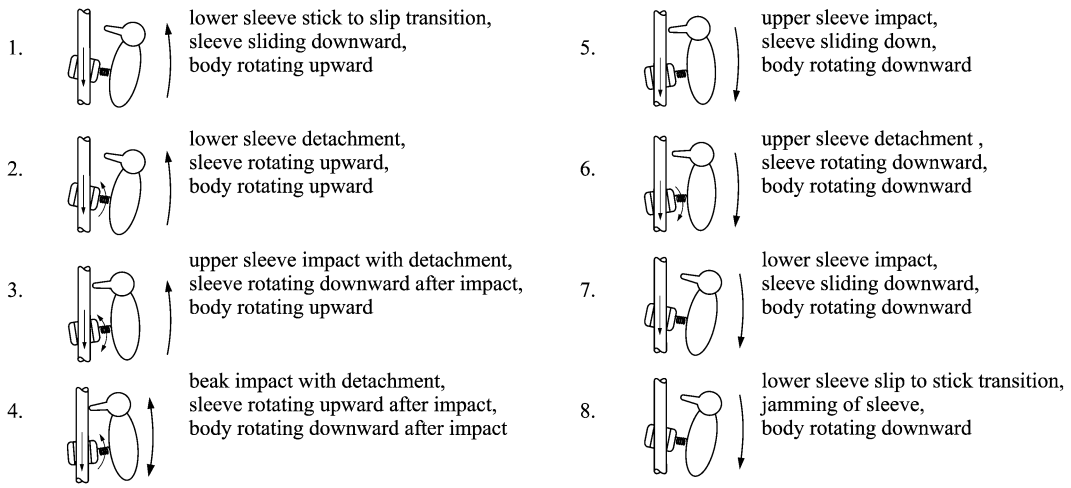


Fig. 14. Sequence of events of the Woodpecker Toy (arrows indicate motion after impact).

observed during this time interval and corresponds to the 72,91 Hz eigenfrequency of the woodpecker–spring–sleeve combination. Impact of the lower sleeve occurs at $t = t_7$, after which the sleeve is sliding down. The woodpecker is rotating downward, increasing the normal force, and jamming of the sleeve starts at $t = t_8$. The succession of sliding and jamming of contact 2 transfers the kinetic energy of the translational motion in $y$ direction, obtained during free falling, into rotational motion of the woodpecker. The woodpecker therefore swings backward when the lower sleeve contact jams, stores potential energy in the spring and swings forward again, $t = t_1 + T$, which completes the periodic motion. Note that due to the completely filled mass matrix $\boldsymbol{M}$, an impact in one of the constraints affects each of the coordinates, which can be seen by the velocity jumps in the time histories and phase portraits of Figs. 12 and 13.

The system has three degrees of freedom, which sets up a 6-dimensional state space $(\boldsymbol{q}, \boldsymbol{u}) \in \mathbb{R}^6$. However, the differential measure $\mathrm{d}\boldsymbol{u}$ is only dependent on $\boldsymbol{z} = (\varphi_M, \varphi_S, \boldsymbol{u}) \in \mathbb{R}^5$ and not on the vertical displacement $y$. The 6-dimensional system can therefore be looked upon as a set of a 5-dimensional reduced system $\mathrm{d}\boldsymbol{z} \in \mathrm{d}\boldsymbol{F}(\boldsymbol{z})$ and a one-dimensional differential equation $\dot{y} = g(\boldsymbol{z})$. The on average decreasing displacement $y$ can never be periodic. With a periodic solution of the system we mean periodic motion of the 5 states $\boldsymbol{z}$. The reduced system $\mathrm{d}\boldsymbol{z} \in \mathrm{d}\boldsymbol{F}(\boldsymbol{z})$ possesses a set of stationary solutions

$$\varphi_M = \varphi_S, \quad |\varphi_M| \leqslant (r_M - r_0)/h_M = 0.1034, \ \dot{\varphi}_M = \dot{\varphi}_S = 0,$$

which correspond with a free falling motion of the toy along the shaft. This free falling can indeed be observed in the real toy, abruptly ended by the basement on which the shaft is mounted.

During the interval $t_8 < t < t_1 + T$, the sleeve is jamming and the woodpecker achieves a minimum rotation of $\varphi_S = -0.53$ rad. The rotation $\varphi_S$ is the only non-constrained degree of freedom during jamming, which allows for a one-dimensional Poincaré mapping. Consider the one-dimensional hyperplane $\Omega$ as a section of the 5-dimensional reduced phase space defined by

$$\Omega = \left\{(\varphi_M, \varphi_S, \boldsymbol{u}) \in \mathbb{R}^5 \mid \varphi_M = -(r_M - r_0)/h_M, \boldsymbol{u} = \boldsymbol{0}\right\}. \tag{23}$$

If the woodpecker arrives at a local extremum during jamming, then the state $\boldsymbol{z}$ must lie on $\Omega$. From a state $\boldsymbol{z}_k \in \Omega$, a solution evolves which may return to $\Omega$ at $\varphi_S = \varphi_{S_{k+1}}$. We define the one-dimensional first return map $P : \Omega \to \Omega$ as

$$\varphi_{S_{k+1}} = P(\varphi_{S_k}). \tag{24}$$

Periodic solutions and equilibria, which achieve a local extremum during jamming of the sleeve, are fixed points of $P$. Periodic solutions might exist, at least in theory, which do not contain a jamming part during the period (for instance when the friction coefficient $\mu_2$ is small). Those types of solutions cannot be found by means of this Poincaré map. Still, the map $P$ is suitable to study the manufacturers intended operation of the toy, which is a period-1 solution with jamming, and deviations from this periodic motion.

The Poincaré map $P$ for $\varepsilon_{N1} = 0.5$ is shown in Fig. 15, obtained by numerical integration with 1000 initial values of $\varphi_{S_k}$ (uniformly distributed between $-2.5 < \varphi_S < 0.11$). The map appears to be very irregular and shows two distinct dips at $\varphi_S = -1.23$ and $\varphi_S = -0.27$. These initial conditions lead to solutions evolving to the free falling motions along the shaft, and will consequently never return to the hyperplane $\Omega$. Initial conditions around these singularities lead to solutions which fall for some time along the shaft, but finally return to constrained motion and to the section $\Omega$. The kinetic energy, built up during the free fall, causes the woodpecker to swing tremendously backward, which explains the form of the dip: the smaller the return value $\varphi_{S_{k+1}}$, the longer the fall time was. The map has no value at the centre of the dip, because the solution does not return to the Poincaré section. The dips are infinitely deep, but become smaller and steeper near the centre. A finite depth is depicted due to the finite numerical accuracy. The dip at $\varphi_S = -0.27$ consists of solutions which are directly trapped by the falling motion, whereas the left dip consists of solutions which first have an upper-sleeve impact before being trapped. More dips exist left of the depicted domain, all characterised by a sequence of events before the solution comes into free fall.

Several points can be observed in Fig. 15, on which the map is discontinuous (for instance at $\varphi_{S_k} = -0.76$ and $-2.35$). The solution from an initial condition on the section $\Omega$ undergoes a sequence of events (impacts, stick–slip transitions) before return to $\Omega$. The order, type and number of events in the sequence changes for varying initial conditions $\varphi_{S_k}$. When the order of two events changes at a critical initial condition $\varphi_{S_c}$, then a discontinuity in the solution occurs with respect to the initial condition (see Brogliato, 1999, and references therein). This discontinuity

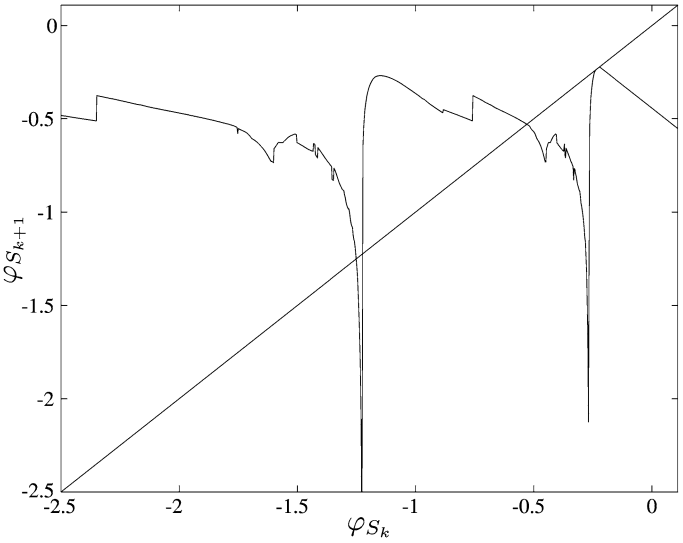


Fig. 15. Poincaré map, $\varepsilon_{N1} = 0.5$.

with respect to initial condition causes discontinuities in the Poincaré map. At the values $\varphi_{S_k} = -0.76$ and $-2.35$ for instance, the order of an upper sleeve impact and a beak impact are interchanged.

The Poincaré map $P$ has been calculated for 94 different values (not uniformly distributed) of the beak restitution coefficient $\varepsilon_{N1}$. A bifurcation diagram was constructed from the set of mappings $P$ by finding the crossings of the maps with the diagonal $\varphi_{S_{k+1}} = \varphi_{S_k}$. Each crossing is, for a locally smooth mapping, a stable or unstable periodic solution or equilibrium. The stability depends on the slope of the mapping at the crossing with the diagonal. The map $P$ is discontinuous and also the jumps in the map can have crossings with the diagonal. Those discontinuous crossings are, however, not periodic solutions or equilibria.

Fig. 16 shows the period-1 solutions of the Woodpecker Toy for varying $\varepsilon_{N1}$. Black lines indicate stable periodic solutions and light gray unstable periodic solutions. The woodpecker can oscillate with small amplitude around the equilibrium point. These solutions are centres, due to the lack of damping between sleeve and woodpecker, and are indicated by a black band in Fig. 16 around the equilibrium at $\varphi_S = -0.2216$. Discontinuous crossings of the map with the diagonal are indicated by dotted lines and connect stable and unstable branches of periodic solutions. There exists a critical initial condition on the Poincaré section for which the solution after some time has two impact events which occur simultaneously (the beak impact and the upper sleeve impact). The order of the impacts changes when the initial condition is changed around this critical initial condition. This gives a discontinuity in the Poincaré map at the fixed value of the critical initial condition. The return values before and after the jump are however dependent on the restitution coefficient. The jump crosses the diagonal for some ranges of the restitution coefficient. These branches of discontinuity crossings are of course straight horizontal lines in Fig. 16 because the critical initial condition is not dependent on the restitution coefficient.

Two stretched islands, $I_1$ and $I_2$, with unstable periodic solutions and discontinuous crossings can be observed in Fig. 16. They are created by the two dips in the Poincaré map (Fig. 15). It should be noted that the bifurcation diagram in Fig. 16 is not complete. Small islands and additional branches of periodic solutions/discontinuous crossings might have been lost by the finite accuracy and the finite domain of the $P$ map. More islands probably exist due to additional dips left of the considered domain.

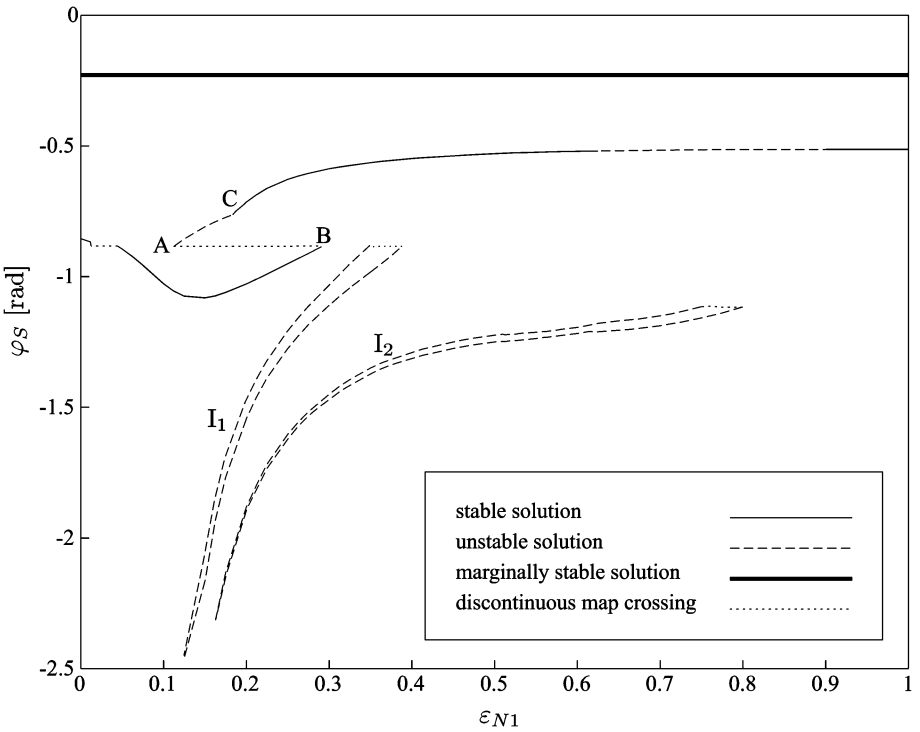


Fig. 16. Bifurcation diagram, period-1 solutions.

From the $P$ maps one can, in theory, construct higher-order maps $P_j$, $j = 2, 3, \ldots$, by mapping $P$ onto itself, but the accuracy of the maps decreases for increasing order due to the finite discretisation of $P$. The set of $P_2$ maps was constructed from the set of maps $P$. Fig. 17 shows the period-2 solutions/discontinuous crossings (and also the period-1 solutions/crossings), obtained by finding the crossings of $P_2$ with the diagonal. Many additional branches appear in Fig. 17, some branches of period-2 solutions, others being discontinuous crossings of $P_2$ with the diagonal. Higher-order branches (3 and higher) most surely also exist, but could not be computed accurately from $P$.

Branches of period-2 solutions appear in Fig. 17 in pairs, as can be expected. It must hold for a period-2 solution that $\varphi_{S_{k+2}} = \varphi_{S_k}$ and $\varphi_{S_{k+3}} = \varphi_{S_{k+1}}$. In general it holds that $\varphi_{S_{k+1}}$ is not equal to $\varphi_{S_k}$ and they therefore appear as two different crossings in the $P_2$ map and as different branches in the bifurcation diagram. The two branches of one pair just contain the same periodic solution but shifted in time.

Very remarkable is that discontinuity crossings of $P_2$ do not appear in pairs, as can be seen for example at point A in Fig. 17. At point A the branch of unstable period-1 solutions turns around and becomes a branch of $P_1$ discontinuity crossings, after which it is folded back to a stable branch at point B. A branch of $P_2$ discontinuity crossings bifurcates from the period-1 branch at A and makes a connection with point C. The $P_2$ discontinuity branch between A and C is clearly single (not a pair). More insight into what exactly happens at the non-conventional bifurcation point A can be gained from a local analysis of the mappings $P$ and $P_2$. Fig. 18 shows a zoom of $P$ and $P_2$ around the crossings of interest for $\varepsilon_{N1} = 0.125$, which is between A and C. The map $P$ is locally discontinuous and crosses the diagonal three times, leading to a stable and unstable periodic solution and a discontinuity crossing. Studying the movement of the map for varying $\varepsilon_{N1}$, the map appeared to shift upward for increasing $\varepsilon_{N1}$. We will now study a simple piecewise linear discontinuous map, which locally approximates the numerically obtained $P$-map.

Consider the piecewise linear mapping, dependent on the constants $a > 1$ and $r$,

$$P^L(x) = \begin{cases} -2 + r, & x \leqslant 0, \\ -ax + r, & x > 0 \end{cases} \tag{25}$$

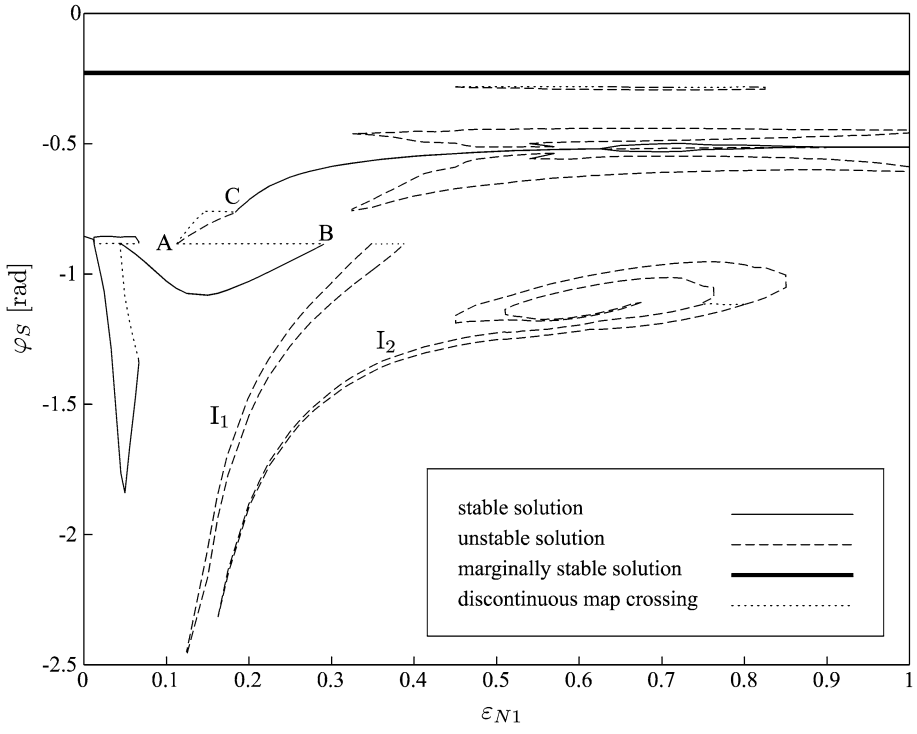


Fig. 17. Bifurcation diagram, period-1 and 2 solutions.

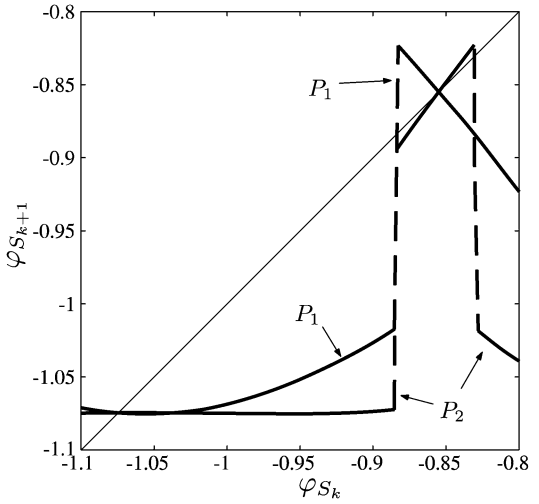


Fig. 18. Zoom of the Poincaré maps for $\varepsilon_{N1} = 0.125$.

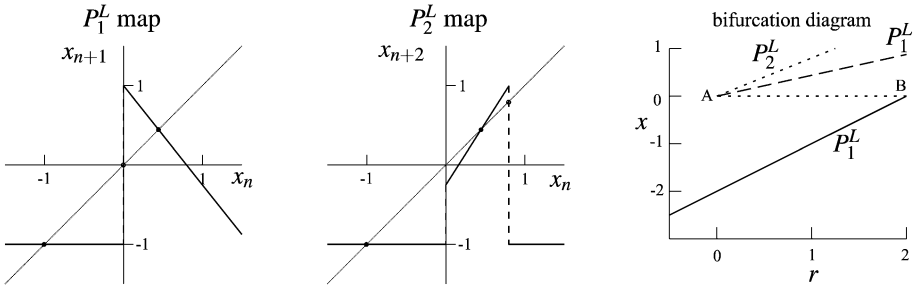


Fig. 19. Analytical analysis of point A in Fig. 17.

which is depicted on the left in Fig. 19 for $a = \frac{5}{4}$ and $r = 1$. The map shifts upward for increasing values of $r$. The map has two regular crossings with the diagonal

$$x = \frac{r}{1+a} > 0, \qquad x = -2 + r < 0$$

for $r > 0$ and $r < 2$ respectively. A discontinuous crossing exists at $x = 0$ for $0 < r < 2$. Mapping $P^L(x)$ onto itself gives $P_2^L(x)$:

$$P_2^L(x) = \begin{cases} -2 + r, & x \leqslant 0, \\ a^2 x + (1-a)r, & 0 < x < \frac{r}{a}, \\ -2 + r, & x \geqslant \frac{r}{a} \end{cases} \tag{26}$$

and is depicted in the middle picture of Fig. 19. The $P_2^L(x)$ map is again piecewise linear in $x$ and has two discontinuities at $x = 0$ and $x = \frac{r}{a}$. The same regular crossings of $P^L$ appear of course in $P_2^L$. Additionally, $P_2^L(x)$ has a *single* discontinuous crossing with the diagonal at $x = \frac{r}{a}$ but does not contain a discontinuous crossing at $x = 0$, like $P^L$. Note that $P^L$ and $P_2^L$ look indeed similar to $P$ and $P_2$ in Fig. 18. Varying $r$ gives the bifurcation diagram depicted in the right of Fig. 19, which is similar to what can be observed in Fig. 17 around point A. Point B is also retrieved from the piecewise linear analysis. The local analysis by the piecewise linear map only predicts the behaviour in a small neighbourhood of point A. The bifurcation at point C is due to other changes in the map $P$ and can therefore not be observed in Fig. 19.

Note that regular crossings of $P^L$ are also regular crossings of $P_2^L$, because they correspond to the periodic solutions and equilibria of the system. Discontinuous crossings of $P^L$ are in general *not* necessarily discontinuous crossings of $P_2^L$. Branches of higher-order discontinuous crossings of $P_j^L$, $j > 2$, also start at point A. It can there-

fore be expected that these branches can also be found for the Woodpecker Toy if the higher-order maps would be calculated accurately.

Bifurcation point A shows behaviour similar to a fold bifurcation, at which a branch is folded around, albeit that the branch changes to a branch of discontinuous crossings after folding. Apart from the folding action, also a branch with $P_2$ discontinuous crossings bifurcate from the period-1 branch at point A. In some sense, this behaviour is similar to a flip or period-doubling bifurcation, at which a period-doubled solution bifurcates form the period-1 branch. The bifurcation point A therefore shows both folding and a kind of flip action. This is not in conformity with the bifurcation theory for smooth systems, which predicts that bifurcations are either fold or flip bifurcations (or of other type). Bifurcation point A is therefore a non-conventional bifurcation point. A similar bifurcation point, showing both fold and flip action, has been found for the system of Filippov-type in Section 3 and is related to the tent map. Note that the $P$ map shows indeed a peak, similar to the tent map, although one flange is vertical.

The nonlinear dynamics of the Woodpecker Toy has been studied in this section. The analysis is not complete, because many other parameters can be varied. The chaotic attractors are also not considered. Still, the variation of $\varepsilon_{N1}$ gives more insight in the complex dynamical phenomena present in the system. A one-dimensional mapping has been found for the Woodpecker Toy. This mapping turns out to be very valuable for the construction of bifurcation diagrams, because it detects not only the periodic solutions but also the discontinuity crossings. Branches of discontinuity crossings appear to connect branches of periodic solutions and are therefore a new kind of objects in the bifurcation diagram, different from attractors. Furthermore, the one-dimensional mapping can be used to gain a better understanding of non-conventional bifurcation points.

## 5. Conclusions

A number of non-smooth dynamical systems of different kind have been studied in the previous sections revealing a variety of bifurcation phenomena that are not encountered in smooth systems. The considered systems are almost always mechanical, but similar bifurcation phenomena occur in for instance non-smooth electrical networks or non-smooth economical models. The term ‘discontinuous bifurcation’ is launched to denote bifurcations that are typical for non-smooth systems.

The bifurcations of equilibria in two planar non-smooth continuous systems have been analysed in Section 2 by using a generalised Jacobian matrix. System (2) shows a discontinuous bifurcation of an equilibrium point at which periodic solutions are created. The complex conjugated eigenvalues of the generalised Jacobian at the bifurcation point form a path through the imaginary axis. Without any problem, we can name this a discontinuous Hopf bifurcation point, due to its resemblance with the classical Hopf bifurcation. The second system (8) also reveals a discontinuous bifurcation, but the path of the generalised eigenvalues crosses the imaginary axis twice: as a complex conjugated pair and one real eigenvalue through the origin. This multiple crossing bifurcation shows a folding action of an equilibrium branch, but the bifurcation phenomenon is far more complex than an classical turning point bifurcation as is also illustrated by the study of a smooth approximation system (14). The latter example demonstrates very well the problem of terminology and classification of discontinuous bifurcations in the class of non-smooth continuous systems. This classification problem of bifurcations becomes even worse when studying classes of systems with discontinuous vector fields or states.

An example of a non-autonomous Filippov system, belonging to the class of differential inclusions, has been studied in Section 3. This system shows a number of remarkable discontinuous bifurcations of periodic solutions. The set-valuedness of the right-hand side can cause the generalised monodromy matrix of a periodic solution to become set-valued. The Floquet multipliers, being the eigenvalues of the (generalised) monodromy matrix, therefore jump or can be considered to be set-valued. The Poincaré maps of Filippov systems are non-smooth but continuous. Their periodic solutions are fixed points of these non-smooth continuous maps and therefore show similar bifurcations as equilibria in non-smooth continuous systems. Of special interest is bifurcation point B, being a multiple crossing bifurcation of a periodic solution for which the path of the generalised Floquet multipliers crosses $+1$ and $-1$. This bifurcation point shows the behaviour of a fold bifurcation and a period doubling bifurcation, but is more complex because infinitely many period-doubled branches are created at the bifurcation point. This bifurcation point has therefore a clear relation to the tent map.

Lastly, the dynamics of the Woodpecker Toy has been analysed by using a one-dimensional Poincaré map method. The Woodpecker Toy is a mechanical example of a system with state discontinuities and can be described by measure

differential inclusions. The unilaterality of the contacts in the system allows for the construction of a one-dimensional map which describes the complete dynamics of the system. Simultaneous impacts in the system lead to a discontinuity of the time-evolution with respect to the initial condition and therefore to discontinuities in the one-dimensional map. The dynamics is greatly influenced by these discontinuities which cause discontinuous bifurcations. The behaviour of bifurcation point A has been analysed in detail by studying analytically a locally similar one-dimensional map. Branches of discontinuity crossings appear to connect branches of periodic solutions (or fixed points) in the bifurcation diagram at discontinuous bifurcation points.

We conclude from the considered examples that a number of analysis tools are available for non-smooth systems, but that we are still far from a complete classification of discontinuous bifurcations. Bifurcations of equilibrium points and sets (Van de Wouw and Leine, 2004), as well as bifurcations of periodic solutions, are closely related to the gain or loss of stability under variation of a system parameter. A clear definition of stability, together with theorems to prove stability (e.g. Lyapunov-type theorems), is quintessential for an in-depth understanding of bifurcations in non-smooth dynamical systems and will be a major topic of further research.

## References


Begley, C.J., Virgin, L.N., 1998. Impact response under the influence of friction. Journal of Sound and Vibration 211 (5), 801–818.

Blazejczyk-Okolewska, B., Kapitaniak, T., 1996. Dynamics of impact oscillator with dry friction. Chaos, Solitons & Fractals 7 (9), 1455–1459.

Brogliato, B., 1999. Nonsmooth Mechanics, second ed.. Springer, London.

Casini, P., Vestroni, F., 2004. Nonstandard bifurcations in oscillators with multiple discontinuity boundaries. International Journal of Nonlinear Dynamics and Chaos in Engineering Systems 35 (1), 41–599.

Clarke, F.H., Ledyaev, Y.S., Stern, R.J., Wolenski, P.R., 1998. Nonsmooth Analysis and Control Theory. Graduate Texts in Mathematics, vol. 178. Springer, New York.

Dankowicz, H., Nordmark, A.B., 2000. On the origin and bifurcations of stick–slip oscillations. Physica D 136 (3–4), 280–302.

di Bernardo, M., Feigin, M.I., Hogan, S.J., Homer, M.E., 1999. Local analysis of C-bifurcations in $n$-dimensional piecewise-smooth dynamical systems. Chaos, Solitons & Fractals 10 (11), 1881–1908.

di Bernardo, M., Garafalo, F., Ianelli, L., Vasca, F., 2002. Bifurcations in piece-wise smooth feedback systems. International Journal of Control 75 (16), 1243–1259.

Elmer, F.-J., 1997. Nonlinear dynamics of dry friction. Journal of Physica A: Mathematical and General 30 (17), 6057–6063.

Feigin, M.I., 1978. On the structure of C-bifurcation boundaries of piecewise-continuous systems. PMM 42 (5), 820–829.

Feigin, M.I., 1995. The increasingly complex structure of the bifurcation tree of a piecewise-smooth system. Journal of Applied Mathematics and Mechanics 59 (6), 853–863.

Filippov, A.F., 1988. Differential Equations with Discontinuous Right-Hand Sides. Kluwer Academic, Dordrecht.

Foale, S., Bishop, R., 1994. Bifurcations in impacting oscillations. International Journal of Nonlinear Dynamics and Chaos in Engineering Systems 6, 285–299.

Galvanetto, U., Knudsen, C., 1997. Event maps in a stick–slip system. International Journal of Nonlinear Dynamics and Chaos in Engineering Systems 13 (2), 99–115.

Glendinning, P., 1994. Stability, Instability and Chaos: An Introduction to the Theory of Nonlinear Differential Equations. Cambridge University Press, Cambridge.

Glocker, Ch., 1995. Dynamik von Starrkörpersystemen mit Reibung und Stößen, Fortschritt-Berichte VDI, vol. 18, no. 182. VDI Verlag, Düsseldorf.

Glocker, Ch., 2001. Set-Valued Force Laws, Dynamics of Non-Smooth Systems. Lecture Notes in Applied Mechanics, vol. 1. Springer-Verlag, Berlin.

Glocker, Ch., Studer, C., 2005. Formulation and preparation for numerical evaluation of linear complementarity systems in dynamics. Multibody System Dynamics 13, 447–463.

Hinrichs, N., Oestreich, M., Popp, K., 1998. On the modelling of friction oscillators. Journal of Sound and Vibration 216 (3), 435–459.

Ivanov, A.P., 1996. Bifurcations in impact systems. Chaos, Solitons & Fractals 7 (10), 1615–1634.

Kunze, M., Küpper, T., 1997. Qualitative bifurcation analysis of a non-smooth friction oscillator model. Zeitschrift für angewandte Mathematik und Physik 48 (1), 87–101.

Leine, R.I. 2000. Bifurcations in discontinuous mechanical systems of Filippov-type, Ph.D. thesis, Eindhoven University of Technology, The Netherlands.

Leine, R.I., Nijmeijer, H., 2004. Dynamics and Bifurcations of Non-Smooth Mechanical Systems. Lecture Notes in Applied and Computational Mechanics, vol. 18. Springer-Verlag, Berlin.

Leine, R.I., Van Campen, D.H., 2002. Discontinuous fold bifurcations in mechanical systems. Archive of Applied Mechanics 72, 138–146.

Leine, R.I., Van Campen, D.H., Van de Vrande, B.L., 2000. Bifurcations in nonlinear discontinuous systems. International Journal of Nonlinear Dynamics and Chaos in Engineering Systems 23 (2), 105–164.

Leine, R.I., Van Campen, D.H., Keultjes, W.J.G., 2002. Stick–slip whirl interaction in drillstring dynamics. ASME Journal of Vibration and Acoustics 124 (2), 209–220.

Leine, R.I., Glocker, Ch., Van Campen, D.H., 2003. Nonlinear dynamics and modeling of various wooden toys with impact and friction. Journal of Vibration and Control 9 (1), 25–78.

Meijaard, J.P., 1996. A mechanism for the onset of chaos in mechanical systems with motion-limiting stops. Chaos, Solitons & Fractals 7 (10), 1649–1658.

Mihajlović, N., van Veggel, A.A., van de Wouw, N., Nijmeijer, H., 2004. Analysis of friction-induced limit cycling in an experimental drill-string system. ASME Journal of Dynamic Systems, Measurements and Control 126 (4), 706–720.

Molenaar, J., de Weger, J.G., van de Water, W., 2001. Mappings of grazing-impact oscillators. Nonlinearity 14, 301–321.

Moreau, J.J., 1988a. Bounded variation in time. In: Moreau, J.J., Panagiotopoulos, P.D., Strang, G. (Eds.), Topics in Nonsmooth Mechanics. Birkhäuser Verlag, Basel, pp. 1–74.

Moreau, J.J., 1988b. Unilateral contact and dry friction in finite freedom dynamics. In: Moreau, J.J., Panagiotopoulos, P.D. (Eds.), Non-Smooth Mechanics and Applications. In: CISM Courses and Lectures, vol. 302. Springer, Wien, pp. 1–82.

Nordmark, A.B., 1997. Universal limit mapping in grazing bifurcations. Physical Review E 55 (1), 266–270.

Nusse, H.E., York, J.A., 1992. Border-collision bifurcations including "period two to period three" for piecewise smooth systems. Physica D 57, 39–57.

Oancea, V.G., Laursen, T.A., 1998. Investigations of low frequency stick–slip motion: experiments and numerical modelling. Journal of Sound and Vibration 213 (4), 577–600.

Peterka, F., 1996. Bifurcations and transition phenomena in an impact oscillator. Chaos, Solitons & Fractals 7 (10), 1635–1647.

Pfeiffer, F., 1984. Mechanische Systeme mit unstetigen Übergängen. Ingenieur-Archiv 54, 232–240.

Pfeiffer, F., Glocker, Ch., 1996. Multibody Dynamics with Unilateral Contacts. Wiley, New York.

Popp, K., Hinrichs, N., Oestreich, M., 1995. Dynamical behaviour of a friction oscillator with simultaneous self and external excitation. Sādhāna, Academy Proceedings in Engineering Sciences 20 (2–4), 627–654.

Stelter, P., Sextro, W., 1991. Bifurcations in dynamical systems with dry friction. International Series of Numerical Mathematics 97, 343–347.

Van de Vorst, E.L.B. Long term dynamics and stabilization of nonlinear mechanical systems, Ph.D. thesis, Eindhoven University of Technology, The Netherlands, 1996.

Van de Vrande, B.L., Van Campen, D.H., De Kraker, A., 1999. An approximate analysis of dry-friction-induced stick–slip vibrations by a smoothing procedure. International Journal of Nonlinear Dynamics and Chaos in Engineering Systems 19 (2), 157–169.

Van de Wouw, N., Leine, R.I., 2004. Attractivity of equilibrium sets of systems with dry friction. International Journal of Nonlinear Dynamics and Chaos in Engineering Systems 35 (1), 19–39.

Yoshitake, Y., Sueoka, A., 2000. Forced self-excited vibration with dry friction. In: Applied Nonlinear Dynamics and Chaos of Mechanical Systems with Discontinuities. World Scientific (Chapter 10).